

Stealth and equiluminous materials for scattering cancellation and wave diffusion

S. Kuznetsova,^{1,*} J.-P. Groby,² L.M. Garcia-Raffi,³ and V. Romero-García^{2,†}

¹*Laboratoire d'Acoustique de l'Université du Mans (LAUM), UMR CNRS 6613, Institut d'Acoustique - Graduate School (IA-GS), CNRS, Le Mans Université, France*

²*Laboratoire d'Acoustique de l'Université du Mans, LAUM - UMR 6613 CNRS, Le Mans Université, Avenue Olivier Messiaen, 72085 LE MANS CEDEX 9, France*

³*Instituto de Matemática Pura y Aplicada (IUMPA), Universitat Politècnica de València, Camino de vera s/n, 46022, Valencia, Spain.*

(Dated: September 3, 2020)

We report a procedure to design 2-dimensional acoustic structures with prescribed scattering properties. The structures are designed from targeted properties in the reciprocal space so that their structure factors, i.e., their scattering patterns under the Born approximation, exactly follow the desired scattering properties for a set of wavelengths. The structures are made of a distribution of rigid circular cross-sectional cylinders embedded in air. We demonstrate the efficiency of the procedure by designing 2-dimensional stealth acoustic materials with broadband backscattering suppression independent of the angle of incidence and equiluminous acoustic materials exhibiting broadband scattering of equal intensity also independent of the angle of incidence. The scattering intensities are described in terms of both single and multiple scattering formalisms, showing excellent agreement with each other, thus validating the scattering properties of each material.

I. INTRODUCTION

Scattering of waves by a many-body system is an interdisciplinary topic of interest in several branches of science and technology ranging from statistical mechanics or condensed matter to wave physics. When such a system is excited by an incident wave, the incoming energy is both scattered and absorbed by the obstacle. This results in a scattering pattern that is highly dependent on the geometry and size of the scatterer distribution as well as on the frequency-dependent properties of the material of the constituent scatterers. The manipulation of wave scattering has long been a topic of discussion in various classical areas of physics including electromagnetism¹, photonics² and acoustics³, but in recent decades significant attention has been paid to artificial structured media to control waves. Photonic^{4–6} or phononic^{7–9} crystals, hyperuniform and stealth materials^{10–14} as well as metamaterials^{15–18} are just a few examples of many-body systems to control the scattering of the incident wave.

Ordered structures, such as photonic^{4–6} and phononic^{7–9,19} crystals, exhibit multiple overlapping Bragg diffraction peaks and thus peculiar dispersion relations that can serve as efficient tools for the control of wave scattering. Metamaterials are complex structures that can be tuned and reconfigured to control the scattering of the incident wave through the resonance of their constituent building blocks^{9,20,21}. Another way of manipulating wave scattering is offered by disordered structures, in which the phase transition between the wave diffusion and localization regimes occurs due to the interference of the waves scattered in the media^{22,23}. Among the disordered systems, stealth materials are characterized by the stealthiness, i.e. the suppression of the single scattering of the incident radiation for a given subset of wave vectors^{11,12}. Recently, one dimensional

stealth acoustic materials have been numerically and experimentally designed to provide stealthiness on demand robust to losses²⁴. A subclass of stealth materials is given by the stealth hyperuniform materials for which transparency appears in a subset of wave vectors around the origin^{10–14}. The relevance of hyperuniformity appeared in condensed matter physics when classical systems of particles interacting with certain soft long-ranged pair potentials could counterintuitively freeze into hyperuniform states. In other words, these systems were counter to the common expectation that liquids freeze into crystal structures with high symmetry. An increasing interest was focused on stealth hyperuniform materials, or simply on hyperuniform materials, as they have been used to design networks with complete band gaps comparable in size to those of a photonic/phononic crystal, while at the same time maintain statistical isotropy, enabling waveguide geometries not possible with photonic/phononic crystals as well as high-density disordered transparent materials.^{12,25–29} Another important class of disordered many-body systems are equiluminous materials¹², which scatter waves uniformly in all directions. Such omnidirectional diffusion could play an important role in improving room acoustics by avoiding unwanted reflections^{3,30,31}.

Materials with targeted scattering properties are usually designed by inverse methods, i.e., their structure parameters are extracted from the scattering data. Although this approach relies on an ill-posed problem^{32,33}, various material design tools based on targeting the scattering properties of the structure have been implemented in both wave physics and condensed matter. Inverse approach^{34–36} consists in optimizing the inter-particle interactions (thus minimizing some energetic characteristics) leading to self-assembling from a simpler condition. Optimization methods operating in direct space rely

on zero-temperature and near-melting temperature technique to obtain lattice ground state configurations^{34,37–41} and collective-coordinates technique for soft matter and disordered ground states^{42,43}. Usual numerical methods include black-box optimization benchmarking⁴⁴, probabilistic^{45,46} and genetic algorithms^{47,48} to name a few. A flat acoustic lens^{49,50} focusing sound at a pre-defined point, a photonic-crystal-based structure⁵¹ performing requested optical tasks, or a sonic demultiplexing device⁵² spatially separating several wavelengths were designed using a genetic algorithm in conjunction with the multiple scattering theory (MST)^{53,54} to optimize a cluster of scatterers. A 2-dimensional low loss acoustic cloak for air-born sound has also been designed by means of genetic algorithm and simulated annealing⁵⁵. Nonlinear conjugate gradient algorithm has been used to optimize a graded porous medium composed of a periodic arrangement of ordered unit cells to provide the optimal acoustic reflection and transmission⁵⁶. Recently scattering suppression of electromagnetic waves for prescribed wavelengths and directions has been achieved by pre-assigning the scattering properties in the reciprocal space and using generalized Hilbert transform⁵⁷.

In this work, we design disordered 2-dimensional (2D) acoustic structures consisting of rigid circular cross-sectional cylinders embedded in air. These structures are designed to present prescribed scattering properties when excited by a plane wave. We target the information on the scattering pattern in the reciprocal space and use an optimization procedure, which optimizes the positions of scatterers to ensure the targeted scattering properties. A weak scattering approach is followed, which allows us to characterize the system by its structure factor. This factor turns out to be proportional to the scattered intensity and only depends on the scatterer positions when they are identical. Therefore, the optimization procedure finds the distribution of scatterers producing the targeted structure factor values by fixing the scattering properties in the reciprocal space and as a consequence the desired scattering properties. The polar scattering pattern of the optimized distribution of scatterers is first evaluated from the representation of the structure factor in the reciprocal space by using the von Laue formulation. This scattering pattern is then evaluated independently by the MST, which is a self-consistent method accounting for all orders of scattering. Comparison of the results of the two methods allows us to validate the approximation of weak scattering and consequently the results. We apply the proposed approach to design and describe 2D stealth and equiluminous materials showing broadband back-scattering suppression and broadband equally intense scattering respectively, independently of the angle of incidence.

II. SCATTERING IN MANY-BODY SYSTEMS: STRUCTURE FACTOR AND MULTIPLE SCATTERING THEORY

We are interested in the scattering of acoustic waves by structures made of a distribution of N rigid cylindrical scatterers with circular cross-section of identical radius $R_i = R_0$ and located at positions \vec{r}_i with $i = 1, \dots, N$. These N scatterers are embedded in a square area Ω of the direct space of side L . We assume weak scattering, i.e., the amplitude of the scattered field is small compared to that of the incident field. Under this condition, we assume that the Born approximation is satisfied. Strictly speaking, Born approximation corresponds to the case in which the incident field to the i -th cylinder is only composed of the incident wave, i.e. no scattered waves by the other scatterers impinges the i -th scatterer. For the geometries considered in this work, the weak scattering approximation is thus valid for low filling fractions and when the scatterer radii are small compared to the wavelength (see Appendix A for more details).

This discrete system can be characterized by the following scalar function defined in the spatial (direct) domain Ω as

$$\rho(\vec{r}) = f(\vec{r}) * \sum_{i=1}^N \delta(\vec{r} - \vec{r}_i), \quad (1)$$

where $*$ is the convolution operator, $\delta(\vec{x})$ is the Dirac's delta and $f(\vec{r})$ is the transparency of the scatterer, defined without loss of generality as

$$f(\vec{r}) = \begin{cases} 0 & \text{if } |\vec{r}| > R_0, \\ 1 & \text{if } |\vec{r}| \leq R_0. \end{cases} \quad (2)$$

Under these assumptions, the amplitude of the scattered wave is proportional to the spatial Fourier transform of $\rho(\vec{r})$, $\mathcal{FT}(\vec{G})$, where \vec{G} is a vector of the reciprocal space. This follows from the well known theory in optics that the diffraction pattern of a structure is equal to the product of the diffraction pattern of the base element and that of the array⁵⁸. Through this work we assume a time harmonic dependence of the type $e^{-i\omega t}$ where ω the angular frequency. With this, we simply end with

$$\mathcal{FT}(\vec{G}) = f(\vec{G}) \times \sum_{i=1}^N e^{-i\vec{G}\vec{r}_i}. \quad (3)$$

Therefore, the scattered intensity is given by

$$I(\vec{G}) = |f(\vec{G})|^2 \times \sum_{i=1}^N \sum_{j=1}^N e^{-i\vec{G}(\vec{r}_i - \vec{r}_j)}, \quad (4)$$

where $f(\vec{G})$ is known as the atomic structure factor and only depends on the geometry of the scatterer as our scatterers are considered rigid. Thus, the scattered intensity can be simply written as

$$I(\vec{G}) = |f(\vec{G})|^2 NS(\vec{G}), \quad (5)$$

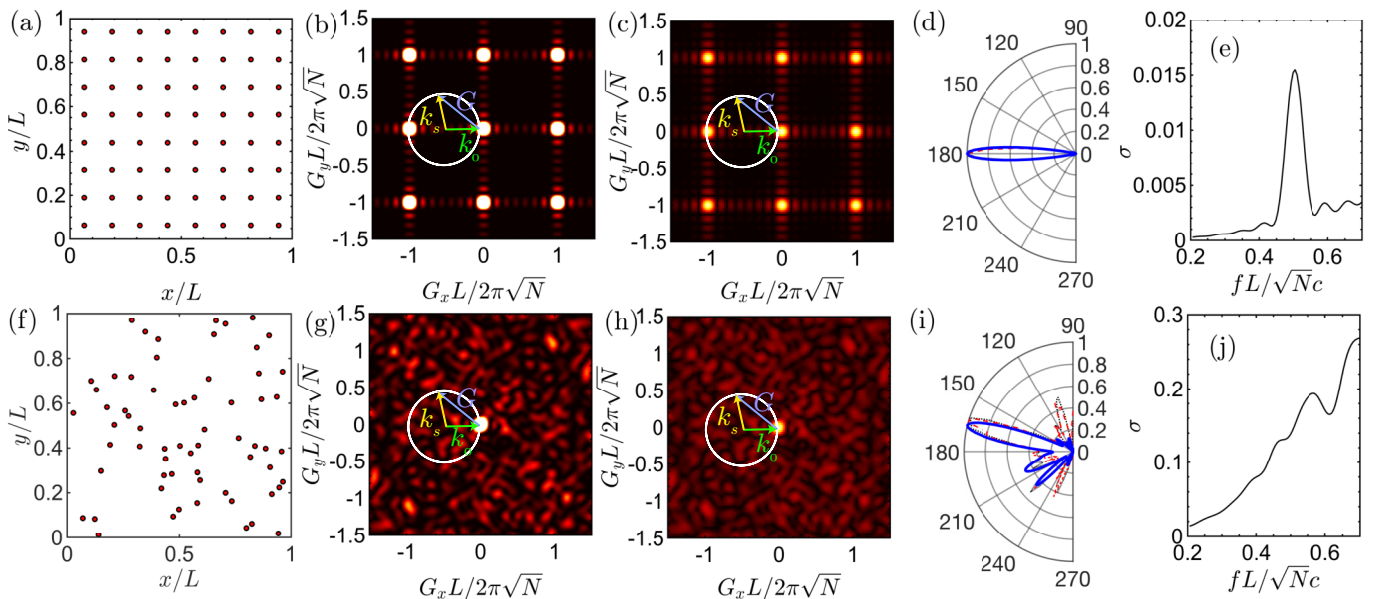


FIG. 1. (Color online) Scattering by an array of N scatterers radiated by an incident plane wave characterized by the wavevector \vec{k}_0 . (a) and (f) represent a periodic and a random distribution of $N = 64$ cylinders with $R_0 = L/100$ respectively.^a (b) and (g) show the representation of the structure factor $S(\vec{G})$ for the periodic and the random distribution respectively. (c) and (h) show the representation of the spatial Fourier transform $|\mathcal{FT}(\vec{G})|$ for the periodic and the random distribution respectively. In (b-c) and (g-h) the incident wavevector and the scattered wavevector are related through the Ewald circumference with the vectors of the reciprocal space. (d) and (i) show the polar distribution of the normalized scattered far field intensity between $\theta = [90, 270]$ degrees for the periodic and the random distributions respectively. Black dotted (red dashed line) [continuous blue line] represents the results obtained from the $S(\vec{G})$ ($|\mathcal{FT}(\vec{G})|^2$) [$|P_s^f(\theta, \omega)|^2$]. (e) and (j) represents the scattering cross section of the periodic and random distributions respectively.

^a The coordinates of these distributions of points are provided in the Supplementary Material

where

$$S(\vec{G}) = \frac{1}{N} \sum_{i=1}^N \sum_{j=1}^N e^{-i\vec{G}(\vec{r}_i - \vec{r}_j)} = \frac{1}{N} \left| \sum_{j=1}^N e^{i\vec{G}\vec{r}_j} \right|^2, \quad (6)$$

is the structure factor. It should be noted here that the structure factor only depends on the position of the scatterers in Ω . Moreover, we notice that $S(\vec{G}) = S(-\vec{G})$ (see Appendix B for more details and additional demonstrations). The structure factor is extensively used in condensed matter or wave physics to describe the scattering of an incident wave by a given structure made of a distribution of scatterers. However, multiple scattering effects are neglected, although this approach has the benefit of allowing fast predictions.

The wave scattering by a distribution of scatterers can effectively be more precisely described by the MST^{53,54}. The far-field expression of the scattered field provided by the MST (see Appendix A for more details) when the structure is radiated by a plane wave with wave vector \vec{k}_0 , is given by

$$p_s^f = P_s^f(\theta, \omega) \sqrt{\frac{k}{i2\pi r}} e^{ikr}, \quad r \rightarrow \infty, \quad (7)$$

where $k = |\vec{k}_0|$ and the far-field scattered amplitude

$P_s^f(\theta, \omega)$, at angle θ , reads as

$$P_s^f(\theta, \omega) = \frac{2}{k} \sum_{i=1}^N e^{-ik|\vec{r}_i| \cos(\theta - \theta_{\vec{r}_i})} \sum_n (-i)^n A_n^i e^{in\theta}, \quad (8)$$

with $\theta_{\vec{r}_i}$, the azimuthal angle of the position vector of the i -th cylinder \vec{r}_i and A_n^i , the scattering coefficients of the i -th cylinder calculated by MST. The scattered far-field intensity is thus proportional to $I(\theta, \omega) \propto |P_s^f(\theta, \omega)|^2$. The scattering cross section of the scatterer distribution when excited by a plane wave e^{ikx} is also computed by applying the Optical Theorem (see Appendix A) via

$$\sigma = -2\text{Re}(P_s^f(0, \omega)) = -\frac{4}{k} \text{Re} \left(\sum_{i=1}^N e^{-ikx_{\vec{r}_i}} \sum_n (-i)^n A_n^i \right). \quad (9)$$

In order to illustrate the different results provided by each method and the interpretation of the scattering in the reciprocal space, the scattering properties of both a periodic and a random distribution of $N = 64$ rigid cylinders of radii $R_0 = L/100$ are analyzed (array of 8×8 rigid cylinders in the periodic case). The random distribution has been generated by choosing random positions of the

scatterers and avoiding overlapping between them. The periodic [random] distribution of scatterers is plotted in Fig. 1(a) [1(f)].⁵⁹ Figures 1(b-c) [1(g-h)] respectively depict $S(\vec{G})$ and $|\mathcal{FT}(\vec{G})|$ in the reciprocal space. In the periodic case, both $S(\vec{G})$ and $\mathcal{FT}(\vec{G})$ consist of a periodic pattern of sinc-type functions. The maxima appear due to the periodicity of the square distribution at $\vec{G} = \left(n\frac{2\pi\sqrt{N}}{L}, m\frac{2\pi\sqrt{N}}{L}\right)$ with $(n, m) \in \mathbb{Z}^2$. In the random case, the representations in the reciprocal space are not periodic as shown in Fig. 1(g-h). In both periodic and random cases, a hot spot in the center that represents the forward scattering is exhibited. The parity of both $S(\vec{G}) = S(-\vec{G})$ and $|\mathcal{FT}(\vec{G})| = |\mathcal{FT}(-\vec{G})|$ is clearly visible.

To interpret the scattering produced by these distributions, we first discuss how the scattering is directly interpreted in the reciprocal space using the von Laue formulation. Let us consider that the system is excited by an incident plane wave the wavevector of which is $\vec{k}_0 = k(\vec{e}_x, 0)$, with \vec{e}_x the unitary vector along the x direction and $k = |\vec{k}_0|$. We choose $k = \pi N/L$ in this particular example to analyze the Bragg scattering in the periodic case. This wavevector \vec{k}_0 is represented in Figs. 1(b-c) [Figs. 1(g-h)] for the periodic [random] case pointing one of the points of the reciprocal space. The von Laue formulation of the wave diffraction⁶⁰ stipulates that the difference between the vector of the scattered wave, \vec{k}_s , and that of the incident wave, must be a vector of the reciprocal space, i.e., $\vec{k}_s - \vec{k}_0 = \vec{G}$, for constructive interference to occur. Assuming elastic scattering, $|\vec{k}_s| \equiv k_s = |\vec{k}_0| = k = 2\pi/\lambda$, only the vectors pointing non zero values of $S(\vec{G})$ along the Ewald sphere⁶⁰ can lead to scattered waves for 3D problems. This sphere of radius k_0 is centered at the origin of \vec{k}_0 in the reciprocal space. More precisely, all the possible scattered waves are given by the Ewald sphere. The scattered wavevectors, \vec{k}_s , are then given by the vector connecting the center of the sphere and the points along this sphere having a non null value of $S(\vec{G})$. The scattering is finally activated along the direction given by these vectors \vec{k}_s . This discussion is valid for any dimension, the Ewald sphere is a circumference in 2D of radius k_0 centred in \vec{k}_0 , and is given by the limits of a segment of length $2k_0$ centred in \vec{k}_0 in 1D.

Following this procedure, the values of $S(\vec{G})$ and $|\mathcal{FT}(\vec{G})|$ along the Ewald circumference between $\theta = [90, 270]$ degrees can be evaluated and, this polar distribution provides the back scattering produced by systems. Figure 1(d) [Figure 1(i)] shows the polar pattern of the scattered field by the periodic [random] distribution. Both $S(\vec{G})$ and $|\mathcal{FT}(\vec{G})|$ present a strong back scattering around 180° as expected from the Bragg scattering. We then compare the results with the scattered far field as calculated by the MST, i.e., when accounting for all the scattering orders. We conclude that

the Bragg scattering is produced and that the results are very close to those given by both $S(\vec{G})$ and $|\mathcal{FT}(\vec{G})|$. For the random scatterer distribution, scattering along more directions than in the periodic case is expected, because more vectors are possible in the reciprocal space. Some directions predicted by both $S(\vec{G})$ and $|\mathcal{FT}(\vec{G})|$ are nevertheless missing when comparing the results with the scattered far field as calculated with the MST. This is due to the fact that scatterers are too close to each other in some area of the distribution for the weak scattering approximation to be valid as shown in Fig. 1(f). In that case, the most realistic modeling is that provided by the MST. However, it should be noted that the main directions of scattering are captured by both $S(\vec{G})$ and $\mathcal{FT}(\vec{G})$.

To conclude this analysis concerning the scattering by a periodic and a random pattern of scatterers, Figs. 1(e) and 1(j) depict the scattering cross section as calculated with the MST for the periodic and the random cases respectively. The Bragg interference produces a peak of scattering at the Bragg frequency $f_{Bragg} = Nc/2L$, where c is the speed of sound in the host fluid material, for the periodic distribution while the scattering cross section almost continuously increases with frequency for the random distribution.

III. MATERIAL DESIGN TOOL

Depending on the values of the structure factor in the reciprocal space, different kinds of materials can be designed¹². In general, the following constraint can be imposed on the structure factor

$$S(\vec{G}) = S_0 \quad \text{for} \quad K_1 \leq |\vec{G}| \leq K_2, \quad (10)$$

where K_1 and K_2 are respectively the lower and the upper limits of an area of the reciprocal space for which $S(\vec{G})$ has a constant value S_0 . Stealth materials present zero structure factor, $S_0 = 0$, for a general set of reciprocal vectors. Hyperuniform materials^{12-14,25-28,61,62} are specific type of stealth materials for which $K_1 = 0$, i.e., infinite-wavelength density fluctuations vanish up to $K_2 = K$. d -dimensional hyperuniform materials are in addition characterized by $\chi = \frac{1}{\pi^{d-1}} \left(\frac{KL}{2N}\right)^d$, which represents the relative fraction of constrained degrees of freedom for a fixed reciprocal-space exclusion-sphere of radius K . Finally, equiluminous materials present a structure factor that is other than zero, i.e., $S_0 \neq 0$ for specified wavevectors in the reciprocal space.

In this section, we present a methodology to design structured materials with prescribed scattering features. In contrast to real-space methods, the desired scattering characteristics are introduced directly in the reciprocal space via the structure factor and an optimization procedure is used to find, the scatter distributions that gives rise to the targeted value of structure factor for a set of wavelengths. The cost function that is minimized during

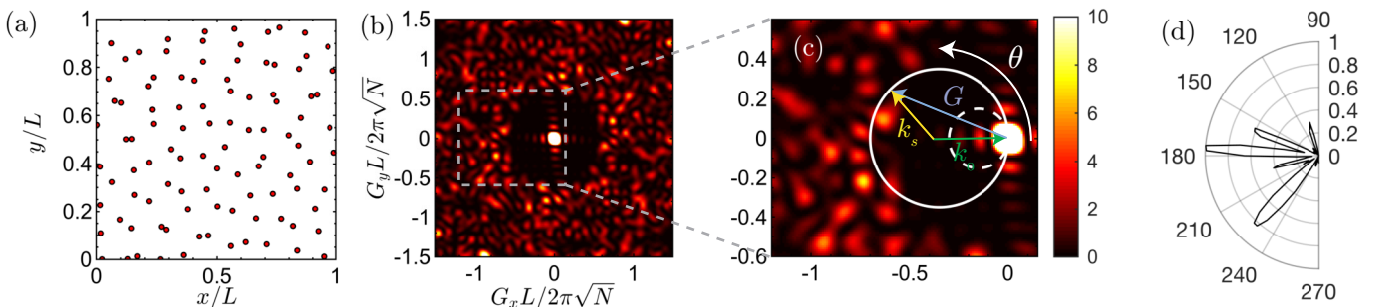


FIG. 2. (Color online) Structure factor and scattering produced by a Hyperuniform material made of $N = 100$ cylinders with $R_0 = L/100$. (a) represents the point distribution for the Hyperuniform material (with $\chi = 0.196$).^a (b) shows the structure factor. (c) is a zoom the region of interest in (b). We plot the Ewald circumference corresponding to an incident wavevector \vec{k}_0 . (d) represents the polar plot of the normalized scattered intensity calculated from the structure factor for the Hyperuniform (at $k_0 = k_s = 0.35 \frac{2\pi\sqrt{N}}{L}$ [white circumference in (c)] between $\theta = [90, 270]$ degrees in order to analyze the back scattering components.

^a The coordinates of this distribution of points are provided in the Supplementary Material

the optimization procedure is a function of the structure factor itself $S(\vec{G})$ [Eq. (6)]. For a given limit of wavevectors, the structure factor must have a target value S_0 for all the wavevectors in domain Λ . The objective function reads as

$$\phi(\vec{r}_1, \dots, \vec{r}_N) = \sum_{\vec{G} \in \Lambda} \left(S(\vec{G}) - S_0 \right), \quad (11)$$

and is subjected to the following constrains to avoid overlapping of scatterers of radius R_0 ,

$$|\vec{r}_i - \vec{r}_j| \geq 2R_0 \quad \forall i \neq j. \quad (12)$$

We note that Eq. (11) is already norm L_2 as $S(\vec{G})$ is already norm L_2 . The optimization algorithm looks for distribution of scatterers \vec{r}_i that minimizes the Eq. (11). Stealth, Hyperuniform, and Equiluminous materials or more generally any kind of materials with targeted properties in the reciprocal space can be designed.

As an example, Figs. 2(a-c) show a hyperuniform material made of a distributions of $N = 100$ rigid cylinders with $R_0 = L/100$ with $\chi = 0.196$ designed by the present procedure.⁶³ Figure 2(b) represents the structure factor of the corresponding scatterer distribution. The scattering suppression area with $S(\vec{G}) = 0$ between $K_1 = 0$ and $K_2 = 0.5 \frac{2\pi\sqrt{N}}{L}$ is clearly visible. Following the discussion on the interpretation of the scattering in the reciprocal space given in Section II, Fig. 2(c) shows the Ewald circumferences for two different incident wavevectors $\vec{k}_0 = (0.35 \frac{2\pi\sqrt{N}}{L} \vec{e}_x, 0)$ (white continuous line) and $\vec{k}_0 = (0.15 \frac{2\pi\sqrt{N}}{L} \vec{e}_x, 0)$ (white dashed line). These two situations correspond respectively to cases where the Ewald circumference is either partially or completely within the scattering suppression area where $S(\vec{G}) = 0$. In both cases, the points along the circumference falling in the region $S(\vec{G}) = 0$ do not produce scattering. For this reason, hyperuniform materials suppress the scattering of incident radiation at low

frequencies. This is the case of the Ewald circumference for $\vec{k}_0 = (0.15 \frac{2\pi\sqrt{N}}{L} \vec{e}_x, 0)$ [white dashed line in Fig. 2(c)]. In the opposite, strong back scattering occurs for $\vec{k}_0 = (0.35 \frac{2\pi\sqrt{N}}{L} \vec{e}_x, 0)$. Figure 2(d) shows the corresponding polar diagrams of the normalized scattered intensities between $\theta = [90, 270]$ degrees as calculated with Eq. (5). The intensity is normalized with respect to its maximum value for $\vec{k}_0 = (0.35 \frac{2\pi\sqrt{N}}{L} \vec{e}_x, 0)$. Therefore, back scattering is clearly exhibited when $\vec{k}_0 = (0.35 \frac{2\pi\sqrt{N}}{L} \vec{e}_x, 0)$ while no back scattering occurs when $\vec{k}_0 = (0.15 \frac{2\pi\sqrt{N}}{L} \vec{e}_x, 0)$. Note that the asymmetry of the polar diagram in Fig. 2(d) around the direction $\theta = 180$ is a direct consequence of the disorder of the scatterer distribution.

IV. RESULTS

In this section we show the results for different materials with targeted scattering properties using the structure factor. We compare the results obtained from the structure factor, the spatial Fourier transform, and the MST.

A. Broadband back-scattering suppression independent of the angle of incidence

We start by analyzing the properties of a stealth material presenting a scattering suppression area between $K_1 = 0.75 \frac{2\pi\sqrt{N}}{L}$ and $K_2 = 1.1 \frac{2\pi\sqrt{N}}{L}$. A distribution of $N = 64$ identical cylindrical rigid scatterers with $R_0 = L/100$ is considered. Figure 3(a) shows the scatterer distribution that minimizes Eq. (11) resulting from the material design tool. Figure 3(b) depicts the corresponding structure factor showing the scattering suppression area between the imposed limits. Note that this particular shape of scattering suppression area im-

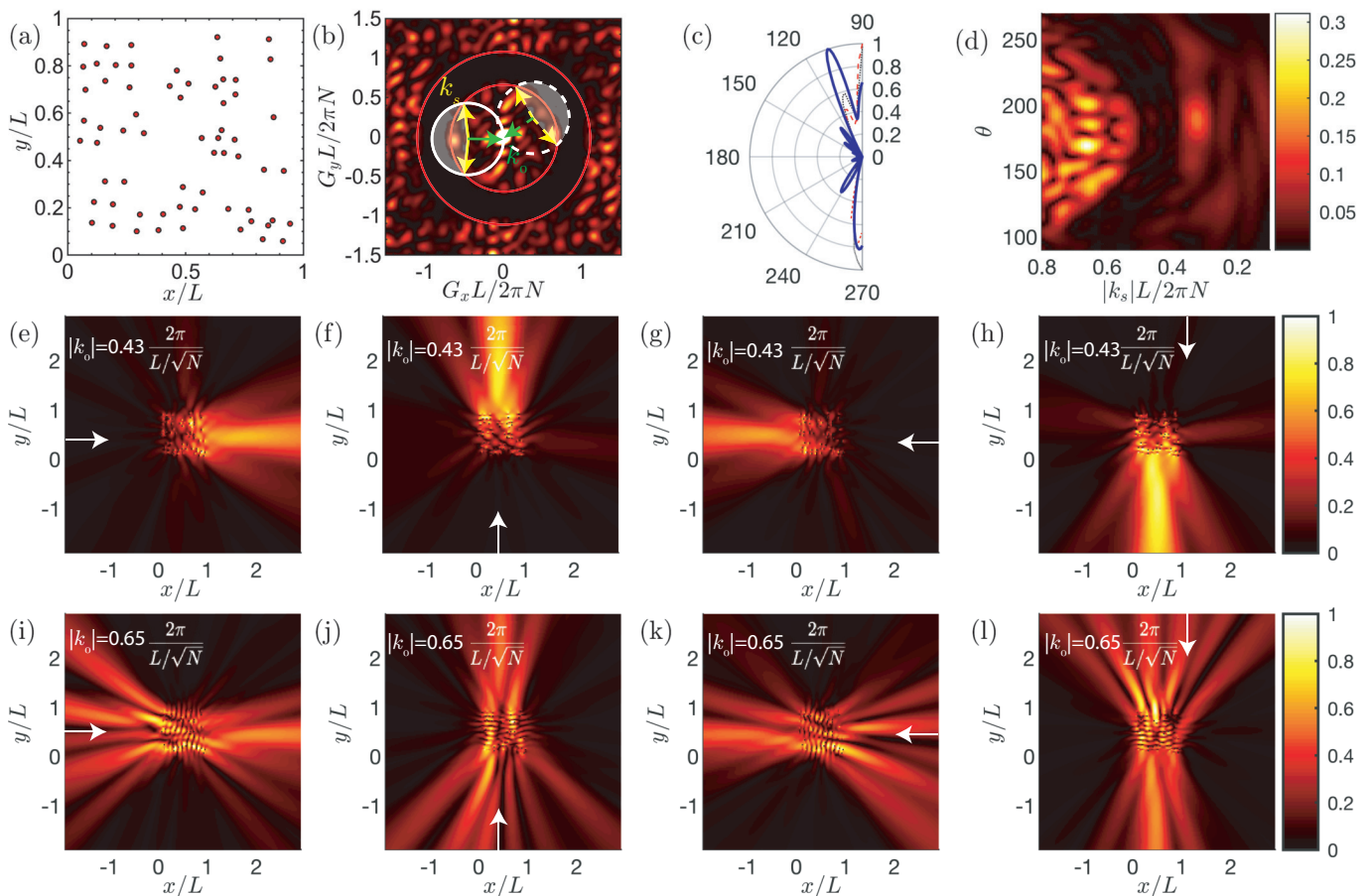


FIG. 3. (Color online) Scattering properties of an stealth material for broadband and omnidirectional back scattering suppression. (a) Stealth distribution.^a (b) Structure factor $S(\vec{G})$ of the stealth material. Ewald circumference distribution for two different incident directions of the same wave. Whitish area shows the scattering suppression for these two examples. Red circles in (b) represent the limits of scattering suppression, $K_1 = 0.75 \frac{2\pi\sqrt{N}}{L}$ and $K_2 = 1.1 \frac{2\pi\sqrt{N}}{L}$. Green (yellow) arrow represents the incident (scattered) plane wave. (c) Polar plot of the scattered field, $|p_s^f(\theta, \omega)|$ produced by this Stealth material obtained from the structure factor (dotted black line), the Fourier transform (dashed red line) and the MST (continuous blue line) for $k = 0.43 \frac{2\pi\sqrt{N}}{L}$. (d) $\theta - |k|$ map of the scattered pressure field $|p_s^f(\theta, \omega)|$ obtained from MST for an incident wavevector $\vec{k}_0 = (0.43 \frac{2\pi\sqrt{N}}{L} \vec{e}_x, 0)$. (e-h) Scattered pressure field $|p_s|$ for an incident wave with $|\vec{k}_0| = 0.43 \frac{2\pi\sqrt{N}}{L}$ (inside the scattering suppression region) along 0° , 270° , 180° , 90° of incidence respectively. (i-l) Normalized scattered pressure field $|p_s|$ for an incident wave with $|\vec{k}_0| = 0.65 \frac{2\pi\sqrt{N}}{L}$ (outside the scattering suppression region) along 0° , 270° , 180° , 90° of incidence respectively.

^a The coordinates of this distribution of points are provided in the Supplementary Material

plies that the back scattering is completely suppressed for any frequency and for any incident wavevector in this area. In Fig. 3(b), two different Ewald circumferences are shown for two different incident directions at the same frequency. The whitish areas represent those of the suppressed scattered wavevectors at this particular frequency. It should be noted here that fixing the frequency of an incident wave having scattered wavevectors in the suppression zone, the suppressed scattering remains the same for any incident direction.

Figure 3(c) shows the polar plot of the scattered field $|p_s^f(\theta, \omega)|$ by this stealth material as calculated with the structure factor (dotted black line), the Fourier transform (dashed red line) and the MST (continuous blue

line) for $\vec{k}_0 = (0.43 \frac{2\pi\sqrt{N}}{L}, 0)$. The back scattering is almost suppressed as evidenced by the polar plot. Figure 3(d) represents the $\theta - |k|$ map of $|p_s^f(\theta, \omega)|$ obtained from the MST. The scattering suppression is clearly in good agreement with the results presented Fig. 3(b). This evidences the broadband back scattering suppression independent of the incident angle.

Figures 3(e-h) finally show the scattered pressure field $|p_s|$ for an incident plane wave with $k_0 = 0.43 \frac{2\pi\sqrt{N}}{L}$ for four different incident directions, $\vec{k}_0 = (k_0, 0)$, $\vec{k}_0 = (0, k_0)$, $\vec{k}_0 = (-k_0, 0)$, and $\vec{k}_0 = (0, -k_0)$ respectively (white arrow). The back scattering components are strongly reduced for each angle of incidence.

As predicted with the Ewald circumference in the

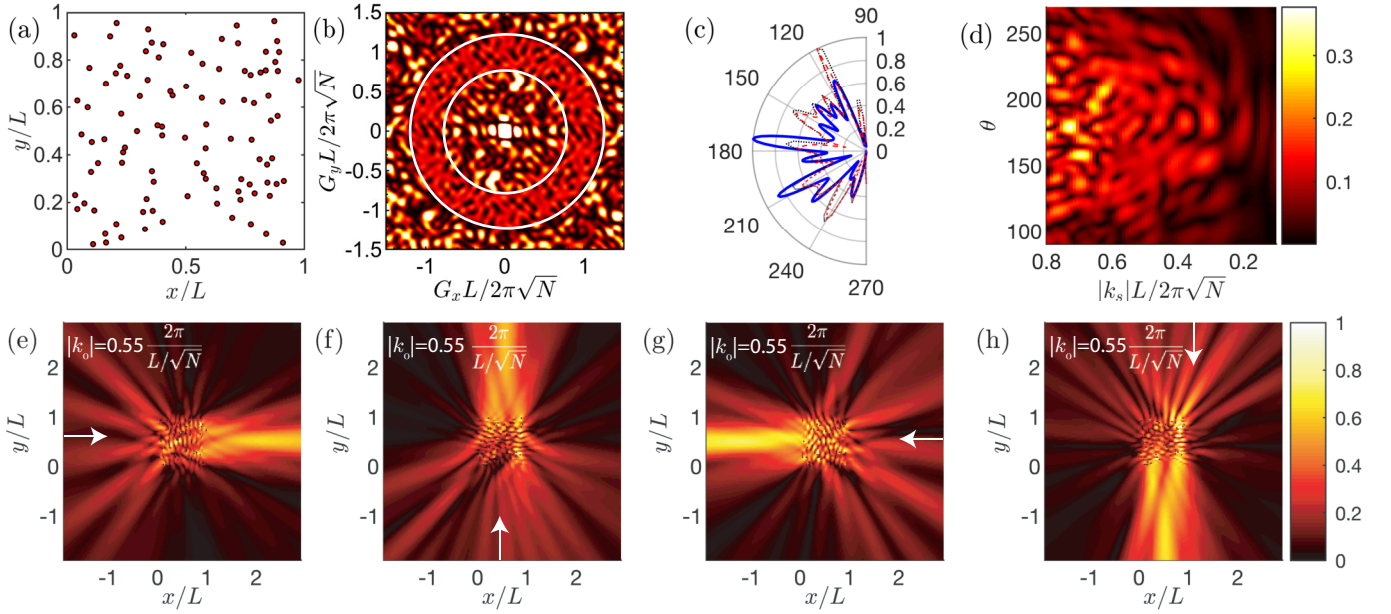


FIG. 4. (Color online) Scattering properties of an equiluminous material for broadband and omnidirectional diffusion. (a) Equiluminous distribution.^a (b) Structure factor $S(\vec{G})$ of the Equiluminous material. White circles in (b) represent the limits of equally intense scattering area, $K_1 = 0.8 \frac{2\pi\sqrt{N}}{L}$ and $K_2 = 1.2 \frac{2\pi\sqrt{N}}{L}$ (with $S_0 = 1$). (c) Polar plot of the scattered field, $|p_s^f(\theta, \omega)|$ produced by this Equiluminous material obtained from the structure factor (dotted black line), the Fourier transform (dashed red line) and the MST (continuous blue line) for $k = 0.55 \frac{2\pi\sqrt{N}}{L}$. (d) $\theta - |k|$ map of the scattered pressure field $|p_s^f(\theta, \omega)|$ obtained from MST for an incident wavevector $\vec{k}_0 = (0.55 \frac{2\pi\sqrt{N}}{L} \vec{e}_x, 0)$. (e-h) Scattered pressure field $|p_s|$ for an incident wave with $|k_0| = 0.55 \frac{2\pi\sqrt{N}}{L}$ (inside the equally intense scattering region) along 0° , 270° , 180° , 90° of incidence respectively.

^a The coordinates of this distribution of points are provided in the Supplementary Material

structure factor map, the forward component is the most important. Although the values of the structure factor, i.e., the scattered intensity, inside the suppression area are not exactly zero, the independence of the back scattering with respect to the incidence angle is still remarkable. In order to prove the strong effect of this back scattering suppression, we show the scattered pressure distribution for a frequency at which the scattered wavevectors fall outside the scattering suppression region. Figures 3(i-l) show the scattered pressure field for $k_0 = 0.65 \frac{2\pi\sqrt{N}}{L}$ at the same incident directions. Both the back scattering and the forward scattering are of equal importance.

B. Broadband equally intense scattering independently of the angle of incidence

Contrary to the stealth materials, we design an equiluminous materials thanks to the proposed material design tool that produce broadband equally intense scattering independent of the angle of incidence. In this section, we discuss an equiluminous material of equally intense scattering area between $K_1 = 0.8 \frac{2\pi\sqrt{N}}{L}$ and $K_2 = 1.2 \frac{2\pi\sqrt{N}}{L}$. For this particular case, and without loss of generality, we consider a distribution of $N = 100$ rigid scatterers with $R_0 = L/100$. Figure 4(a) shows the scatterer distribution

minimizing Eq. (11) with $S_0 = 1$. Figure 4(b) shows the corresponding structure factor showing the equally intense scattering area between the imposed limits [white circles in Fig. 4(a)]. Similarly to the stealth material, this particular shape of equally intense scattering area implies that the back scattering is equally distributed for any frequency and any incident direction (see Fig. 3(b) for the Ewald circumference representation) in this area. Nevertheless, the values of $S(\vec{G})$ inside the equally intense scattering are not completely homogeneous due to the discrete character of the proposed design contrary those of the stealth material. This finds translation in a quasi-equally intense scattering pattern. The values of $S(\vec{G})$ are however clearly smoother inside the target area than outside.

Figure 4(c) depicts the polar plot of the scattered field $|p_s^f(\theta, \omega)|$ by this equiluminous material as calculated with the structure factor (dotted black line), the Fourier transform (dashed red line) and the MST (continuous blue line) for $k = 0.55 \frac{2\pi\sqrt{N}}{L}$. Contrary to the stealth material, the back scattering is almost evenly distributed along the angles and quasi-equally intense as evidenced by the polar plot. Figure 4(d) represents the $\theta - |k|$ map of $|p_s^f(\theta, \omega)|$ obtained from the MST. The quasi-equally intense scattering is in good agreement with the results plotted in Fig. 4(b). This evidences the broadband back

scattering behaviour of the structure independent of the incident angle.

Figures 4(e-h) show the scattered pressure field $|p_s|$ for an incident wave with $k_0 = 0.55 \frac{2\pi\sqrt{N}}{L}$ for four different incident directions, $\vec{k}_0 = (k_0, 0)$, $\vec{k}_0 = (0, k_0)$, $\vec{k}_0 = (-k_0, 0)$, and $\vec{k}_0 = (0, -k_0)$ respectively. The back scattering components are angularly distributed with quasi-equal intensity for each angle of incidence. Although the values of the structure factor, i.e., the scattered intensity, inside the equally intense scattering area are not exactly constant, the quasi-equal intense back scattering independent of the angle of incidence is still remarkable.

V. CONCLUSIONS

Heterogeneous materials formed by a set of scatterers embedded in a host material with tailored properties are a useful tool for the control and manipulation of acoustic, electromagnetic and matter waves. In this work, we present a methodology based on prescribing the scattering properties of the system in the reciprocal space, i.e., prescribing its structure factor, to later obtain the spacial distribution of scatterers with the corresponding scattering properties. The developed methodology was applied to construct stealth and equiluminous materials. The scattered intensity was first obtained from the structure factor based on their proportionality in the weak scattering approximation. The results were validated using the multiple scattering approach that accounts for all the scattering orders. The scattered intensity patterns obtained by these two approaches are in excellent agreement having similar angular distributions. First we have designed a stealth system that exhibits broadband back-scattering suppression independently of the incidence directions, having zero structure factor in the given frequency range and as a consequence, a close to zero scattered intensity. Second, we have designed an equiluminous system that provides broadband diffusion independently of the incident direction, having non zero constant structure factor in the desired range of frequencies. Although the scattered intensity is not exactly the same at different scattering angles (we have a discrete distribution of scatterers), the scattering pattern is still quasi-intense and is smoother inside the target frequency range than outside it. The proposed methodology has proved itself as a powerful tool to design and characterize disordered many-body systems with preassigned scattering properties.

Appendix A: Multiple Scattering Theory

We consider that the N cylinders of radius R_i are located at \vec{r}_i with $i = 1, \dots, N$ to form the distribution in the $x - y$ plane. The system is excited by a plane wave

of the form $p_0(\vec{r}) = e^{ikx}$ with a temporal dependence of the type $e^{-i\omega t}$. The scattered wave by the i -cylinder can be written as

$$p_s(\vec{r}, \vec{r}_i) = \sum_n A_n^i H_n(k|\vec{r} - \vec{r}_i|) e^{in\theta(\vec{r} - \vec{r}_i)}, \quad (\text{A1})$$

where H_n is the n -th order Hankel function of first type. The total field incident to i -th cylinder $p_{in}^i(\vec{r})$ is a superposition of the direct contribution from the incident wave $p_0(\vec{r})$ and the scattered waves from all the other scatterers

$$p_{in}^i(\vec{r}) = p_0(\vec{r}) + \sum_{j=1, j \neq i}^N p_s(\vec{r}, \vec{r}_j). \quad (\text{A2})$$

This incident wave on the i -th cylinder can be expressed as follows

$$p_{in}^i(\vec{r}) = \sum_n B_n^i J_n(k|\vec{r} - \vec{r}_i|) e^{in\theta_{\vec{r} - \vec{r}_i}}, \quad (\text{A3})$$

where J_n is the n -th order Bessel function of first type. We now express the scattered field by the i -th cylinder in the vicinity of the j -th cylinder. To do so, we use the Graff's theorem:

$$p_s(\vec{r}, \vec{r}_j) = \sum_n C_n^{j,i} J_n(k|\vec{r} - \vec{r}_j|) e^{in\theta_{\vec{r} - \vec{r}_j}}, \quad (\text{A4})$$

$$\forall |\vec{r} - \vec{r}_j| \in [R_j, |\vec{r}_j - \vec{r}_i| - R_i], \quad (\text{A5})$$

with

$$C_n^{j,i} = \sum_l A_l^j H_{l-n}(k|\vec{r}_i - \vec{r}_j|) e^{i(l-n)\theta_{\vec{r}_i - \vec{r}_j}}. \quad (\text{A6})$$

The incident plane wave is then represented in the i -th cylinder coordinate system, via

$$p_0(\vec{r}) = e^{ikx} = e^{ikx_j} e^{ik|\vec{r} - \vec{r}_j| \cos(\theta_{\vec{r} - \vec{r}_j})}. \quad (\text{A7})$$

At this stage, we use the Jacobi-Anger expansion to expand the term $e^{ik|\vec{r} - \vec{r}_j| \cos(\theta_{\vec{r} - \vec{r}_j})}$ upon Bessel functions:

$$e^{ik|\vec{r} - \vec{r}_j| \cos(\theta_{\vec{r} - \vec{r}_j})} = \sum_n i^n J_n(k|\vec{r} - \vec{r}_j|) e^{i\theta_{\vec{r} - \vec{r}_j}}. \quad (\text{A8})$$

Therefore, we end with

$$p_0(\vec{r}) = \sum_n S_n^i J_n(k|\vec{r} - \vec{r}_j|) e^{i\theta_{\vec{r} - \vec{r}_j}}, \quad (\text{A9})$$

where

$$S_n^i = i^n e^{ikx_j}. \quad (\text{A10})$$

The factor e^{ikx_j} plays the role of a complex amplitude which depends on the horizontal projection of the position of the j -th scatterer, x_j .

Now that we have expressed all the acoustic fields involved in the problem in the vicinity of the i -th cylinder, we can obtain the following system of equations:

$$B_n^i = S_n^i + \sum_{j=1, j \neq i}^N \sum_l A_l^j H_{l-n}(k|\vec{r}_i - \vec{r}_j|) e^{i(l-n)\theta_{\vec{r}_i - \vec{r}_j}}. \quad (\text{A11})$$

At this stage, the S_n are known, but both B_n and A_l are unknown. The rigid boundary condition provides another equation relating them. At the interface of the i -th cylinder, we have

$$\frac{1}{\rho_0} \frac{\partial p_{ext}}{\partial r} \Big|_{r=R_i} = 0, \quad (\text{A12})$$

giving rise to

$$B_n^i = -\frac{H'_n(kR_i)}{J'_n(kR_i)} A_n^i \equiv \Gamma_n^i A_n^i, \quad (\text{A13})$$

where the primes represent derivative. Therefore the amplitudes of the scattered and the incident fields on the i -th cylinder can be related by means of Γ_n^i .

Finally the system of equations can be written as follows,

$$\Gamma_n^i A_n^i - \sum_{j=1, j \neq i}^N \sum_l G_{n,l}^{j,i} A_l^j = S_n^i, \quad (\text{A14})$$

where

$$G_{n,l}^{j,i} = H_{l-n}(k|\vec{r}_i - \vec{r}_j|) e^{i(l-n)\theta_{\vec{r}_i - \vec{r}_j}} \text{ for } i \neq j. \quad (\text{A15})$$

This system of equations is solved for every frequency by truncating the infinite sums. A good estimation for this truncation is

$$l = n = \text{floor} \left(kR_{max} + 4.05(kR_{max})^{1/3} \right) + 10, \quad (\text{A16})$$

with $R_{max} = \max(R_i)$. Once the system is solved, the coefficients A_n^i are known and the total pressure can be obtained from

$$p(\vec{r}) = e^{i\omega r \cos \theta} + \sum_{i=1}^N \sum_n A_n^i H_n(k|\vec{r} - \vec{r}_i|) e^{in\theta(\vec{r} - \vec{r}_i)}. \quad (\text{A17})$$

1. Scattering cross section

From the previous equations, the expression of the scattering cross section of an array of scatterers can be obtained. The scattered pressure field by a distribution of scatterers can be written as

$$p_s(\vec{r}) = \sum_{i=1}^N \sum_n A_n^i H_n(k|\vec{r} - \vec{r}_i|) e^{in\theta(\vec{r} - \vec{r}_i)}. \quad (\text{A18})$$

In the far field, we have

$$H_n(k|\vec{r} - \vec{r}_j|) \simeq \sqrt{\frac{k}{i2\pi|\vec{r}|}} (-i)^n e^{ik|\vec{r}|} e^{-ik|\vec{r}_j| \cos(\theta - \theta_{\vec{r}_j})}, \quad (\text{A19})$$

considering that $|\vec{r} - \vec{r}_j| \simeq |\vec{r}| - |\vec{r}_j| \cos(\theta - \theta_{\vec{r}_j})$. The far-field scattered pressure expression is also

$$p_s^f = S(\theta, \omega) \sqrt{\frac{k}{i2\pi r}} e^{ikr}, \quad r \rightarrow \infty, \quad (\text{A20})$$

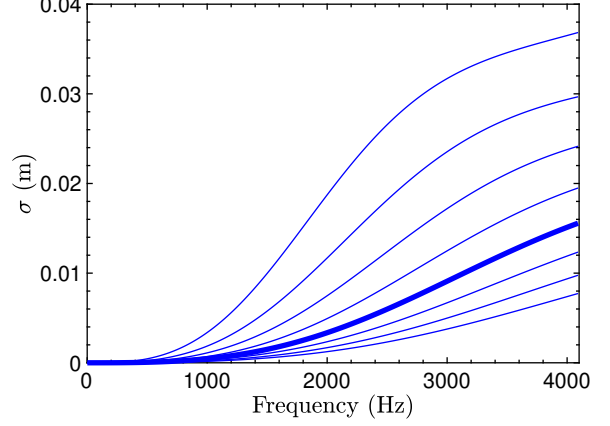


FIG. 5. Scattering cross sections for cylinders with radius $[1/130, 1/120, 1/110, 1/100, 1/90, 1/80, 1/70, 1/60]$. As the radius increases the scattering cross section increases also. The wide line corresponds to the scattering cross section of the cylinders analyzed in this work.

with the far-field scattered amplitude

$$S(\theta, \omega) = \frac{2}{k} \sum_{i=1}^N e^{-ik|\vec{r}_i| \cos(\theta - \theta_{\vec{r}_i})} \sum_n (-i)^n A_n^i e^{in\theta}. \quad (\text{A21})$$

The scattering cross section is thus written as

$$\sigma = -2\text{Re}(S(0, \omega)) = -\frac{4}{k} \text{Re} \sum_{i=1}^N e^{-ikx_{\vec{r}_i}} \sum_n (-i)^n A_n^i. \quad (\text{A22})$$

2. Weak scattering approximation

Strictly speaking the Born approximation implies that the interaction between the scatterers is negligible, in other words, the term $p_s(\vec{r}, \vec{r}_j) = 0$ in Eq. (A2), i.e., the incident wave on the i -th cylinder is only the incident wave without any contribution of the other scatterers in the structure. In this work, we will consider that $|p_s(\vec{r}, \vec{r}_j)| \ll |p_0(\vec{r})| \forall j$. For a single scatterer, the scattering cross section, is defined as

$$\sigma = \frac{1}{|p_0|^2} \int |p_s|^2 ds = \oint \frac{d\sigma}{d\Omega} d\Omega, \quad (\text{A23})$$

where the integral runs over a closed surface enclosing the scatterer. This could be used to evaluate the intensity of the scattered field by a single element. Figure 5 shows the scattering cross section for scatterers with radius $[1/130, 1/120, 1/110, 1/100, 1/90, 1/80, 1/70, 1/60]$. We have chosen a configuration for which the scattering cross section is less than 0.015 in the range of frequencies analyzed in the work, meaning that the scattering is thus 1.5% of the incident wave, so the weak scattering approximation is valid.

Appendix B: Structure factor

Let us consider the scattering of an acoustic beam of wavelength λ by the distribution of N scatterers. We assume that the scattering is weak, so that the amplitude of the incident beam is higher than the amplitude of the scattering waves; absorption, refraction and higher order scattering can be neglected (kinematic diffraction). The direction of any scattered wave is defined by its scattering vector $\vec{G} = \vec{k}_s - \vec{k}_0$, where \vec{k}_s and $\vec{k}_0 = k_0(\cos\theta^i, \sin\theta^i)$ are the scattered and incident beam wavevectors with θ^i the incidence angle. For elastic scattering, $|\vec{k}_s| = |\vec{k}_0| = |\vec{k}| = 2\pi/\lambda$ and then $G = |\vec{G}| = \frac{4\pi}{\lambda} \sin(\theta)$. The amplitude and phase of this scattered wave is the vectorial sum of the scattered waves by all the scatterers $\Psi_s(\vec{q}) = \sum_{i=1}^N f_i e^{-i\vec{G}\vec{r}_i}$, with f_i the atomic structure factor. The scattered intensity reads as

$$\begin{aligned} I(\vec{G}) &= \Psi_s(\vec{G}) \cdot \Psi_s^*(\vec{G}) \\ &= \sum_{j=1}^N f_j e^{-i\vec{G}\vec{r}_j} \times \sum_{k=1}^N f_k e^{i\vec{G}\vec{r}_k} \\ &= \sum_{j=1}^N \sum_{k=1}^N f_j f_k e^{-i\vec{G}(\vec{r}_j - \vec{r}_k)}. \end{aligned} \quad (\text{B1})$$

The structure factor, $S(\vec{G})$, is then defined as this intensity normalized by $1/\sum_{j=1}^N f_j^2$

$$S(\vec{G}) = \frac{1}{\sum_{j=1}^N f_j^2} \sum_{j=1}^N \sum_{k=1}^N f_j f_k e^{-i\vec{G}(\vec{r}_j - \vec{r}_k)}. \quad (\text{B2})$$

If all the scatterers are identical, then

$$I(\vec{G}) = f^2 \sum_{j=1}^N \sum_{k=1}^N e^{-i\vec{G}(\vec{r}_j - \vec{r}_k)}, \quad (\text{B3})$$

so

$$S(\vec{G}) = \frac{1}{N} \sum_{j=1}^N \sum_{k=1}^N e^{-i\vec{G}(\vec{r}_j - \vec{r}_k)} = \frac{1}{N} \left| \sum_{j=1}^N e^{i\vec{G}\vec{r}_j} \right|^2 \quad (\text{B4})$$

Therefore, the structure factor $S(\vec{G})$ is proportional to the intensity of scattered field by a configuration of N scatterers. It is worth noting here that the structure factor can be also related to the scattering cross section as follows

$$\frac{d\sigma}{d\Omega} = f^2 \sum_{j=1}^N \sum_{k=1}^N e^{-i\vec{G}(\vec{r}_j - \vec{r}_k)} = f^2 N S(\vec{G}), \quad (\text{B5})$$

where σ is the total cross-section and Ω is the solid angle.

Note that the von Laue condition^{60,64} for the periodic systems implies that the constructive interferences will occur if the difference between the incident and reflected wavevector is a vector of the reciprocal lattice. Therefore the Bragg scattering condition reads as $|\vec{k}| = \frac{|\vec{G}|}{2 \sin \theta}$. In the 1D case ($\theta = \pi/2$), the wavevectors are collinear and then, $|\vec{k}| = |\vec{G}|/2$.

* svetlana.kuznetsova@univ-lemans.fr

† vicente.romero@univ-lemans.fr

¹ Carl Pfeiffer and Anthony Grbic, “Metamaterial Huygens’ surfaces: Tailoring wave fronts with reflectionless sheets,” *Phys. Rev. Lett.* **110**, 197401 (2013).

² Yifei Zhang, Jeffrey B. Chou, Junying Li, Huashan Li, Qingyang Du, Anupama Yadav, Si Zhou, Mikhail Y. Shalaginov, Zhuoran Fang, Huikai Zhong, Christopher Roberts, Paul Robinson, Bridget Bohlin, Carlos Ríos, Hongtao Lin, Myungkoo Kang, Tian Gu, Jamie Warner, Vladimir Liberman, Kathleen Richardson, and Juejun Hu, “Broadband transparent optical phase change materials for high-performance nonvolatile photonics,” *Nature Communications* **10**, 4279 (2019).

³ Noé Jiménez, Trevor J. Cox, Vicent Romero-García, and Jean-Philippe Groby, “Metadiffusers: Deep-subwavelength sound diffusers,” *Scientific Reports* **7**, 5389 (2017).

⁴ Eli Yablonovitch, “Inhibited spontaneous emission in solid-state physics and electronics,” *Phys. Rev. Lett.* **58**, 2059–2062 (1987).

⁵ Sajeev John, “Strong localization of photons in certain disordered dielectric superlattices,” *Phys. Rev. Lett.* **58**, 2486–2489 (1987).

⁶ John D. Joannopoulos, Steven G. Johnson, Joshua N. Winn, and Robert D. Meade, “Molding the flow of light,” Princeton Univ. Press, Princeton, NJ [ua] (2008).

⁷ M.M. Sigalas and E.N. Economou, “Elastic and acoustic wave band structure,” *Journal of Sound and Vibration* **158**, 377 – 382 (1992).

⁸ R. Martínez-Sala, J. Sancho, J. V. Sánchez, V. Gómez, J. Llinares, and F. Meseguer, “Sound attenuation by sculpture,” *Nature* **378**, 241–241 (1995).

⁹ Pierre A Deymier, *Acoustic metamaterials and phononic crystals*, Vol. 173 (Springer Science & Business Media, 2013).

¹⁰ Obioma U Uche, Frank H Stillinger, and Salvatore Torquato, “Constraints on collective density variables: Two dimensions,” *Physical Review E* **70**, 046122 (2004).

¹¹ S. Torquato, “Random Heterogeneous Materials: Microstructure and Macroscopic Properties,” *Ap-*

- plied *Mechanics Reviews* **55**, B62–B63 (2002), https://asmedigitalcollection.asme.org/appliedmechanicsreviews/pdf/55/4/B62/5439035/b61_1.pdf.
- 12 Robert D. Batten, Frank H. Stillinger, and Salvatore Torquato, “Classical disordered ground states: Super-ideal gases and stealth and equi-luminous materials,” *Journal of Applied Physics* **104**, 033504 (2008), <https://doi.org/10.1063/1.2961314>.
 - 13 Salvatore Torquato, “Hyperuniformity and its generalizations,” *Phys. Rev. E* **94**, 022122 (2016).
 - 14 S. Torquato, G. Zhang, and F. H. Stillinger, “Ensemble theory for stealthy hyperuniform disordered ground states,” *Phys. Rev. X* **5**, 021020 (2015).
 - 15 Nader Engheta and Richard W Ziolkowski, *Metamaterials: physics and engineering explorations* (John Wiley & Sons, 2006).
 - 16 Zhengyou Liu, Xixiang Zhang, Yiwei Mao, Y. Y. Zhu, Zhiyu Yang, C. T. Chan, and Ping Sheng, “Locally resonant sonic materials,” *Science* **289**, 1734–1736 (2000), <https://science.sciencemag.org/content/289/5485/1734.full.pdf>.
 - 17 Nicholas Fang, Dongjuan Xi, Jianyi Xu, Muralidhar Ambati, Wera Yut Srituravanich, Cheng Sun, and Xiang Zhang, “Ultrasonic metamaterials with negative modulus,” *Nature Materials* **5**, 452–456 (2006).
 - 18 Zi Jing Wong, Yuan Wang, Kevin O’Brien, Junsuk Rho, Xiaobo Yin, Shuang Zhang, Nicholas Fang, Ta-Jen Yen, and Xiang Zhang, “Optical and acoustic metamaterials: superlens, negative refractive index and invisibility cloak,” *Journal of Optics* **19**, 084007 (2017).
 - 19 Jean-Philippe Groby and Dominique Lesselier, “Localization and characterization of simple defects in finite-sized photonic crystals,” *J. Opt. Soc. Am. A* **25**, 146–152 (2008).
 - 20 R.V. Craster and S. Guenneau, *Acoustic Metamaterials, vol. 166 of Springer Series in Materials Science* (Springer, 2013).
 - 21 V. Romero-García and A.C. Hladky-Hennion, *Fundamentals and Applications of Acoustic Metamaterials: From Seismic to Radio Frequency* (ISTE Wiley, 2019).
 - 22 Diederik S. Wiersma, Paolo Bartolini, Ad Lagendijk, and Roberto Righini, “Localization of light in a disordered medium,” *Nature* **390**, 671–673 (1997).
 - 23 Hefei Hu, A. Strybulevych, J. H. Page, S. E. Skipetrov, and B. A. van Tiggelen, “Localization of ultrasound in a three-dimensional elastic network,” *Nature Physics* **4**, 945–948 (2008).
 - 24 V. Romero-García, N. Lamothe, G. Theocharis, O. Richoux, and L.M. García-Raffi, “Stealth acoustic materials,” *Phys. Rev. Applied* **11**, 054076 (2019).
 - 25 G. Gkantzounis, T. Amoah, and M. Florescu, “Hyperuniform disordered phononic structures,” *Phys. Rev. B* **95**, 094120 (2017).
 - 26 Marian Florescu, Salvatore Torquato, and Paul J. Steinhardt, “Designer disordered materials with large, complete photonic band gaps,” *Proceedings of the National Academy of Sciences* **106**, 20658–20663 (2009), <https://www.pnas.org/content/106/49/20658.full.pdf>.
 - 27 Weining Man, Marian Florescu, Eric Paul Williamson, Yingquan He, Seyed Reza Hashemizad, Brian Y. C. Leung, Devin Robert Liner, Salvatore Torquato, Paul M. Chaikin, and Paul J. Steinhardt, “Isotropic band gaps and freeform waveguides observed in hyperuniform disordered photonic solids,” *Proceedings of the National Academy of Sciences* **110**, 15886–15891 (2013), <https://www.pnas.org/content/110/40/15886.full.pdf>.
 - 28 Weining Man, Marian Florescu, Kazue Matsuyama, Polin Yadak, Geev Nahal, Seyed Hashemizad, Eric Williamson, Paul Steinhardt, Salvatore Torquato, and Paul Chaikin, “Photonic band gap in isotropic hyperuniform disordered solids with low dielectric contrast,” *Opt. Express* **21**, 19972–19981 (2013).
 - 29 L. Froufe, M. Engel, J. Sáenz, and F. Scheffold, “Band gap formation and anderson localization in disordered photonic materials with structural correlations,” *Proceedings of the National Academy of Sciences* **114**, 201705130 (2017).
 - 30 Trevor J Cox and Peter D’antonio, *Acoustic absorbers and diffusers: theory, design and application* (Crc Press, 2009).
 - 31 Yifan Zhu, Xudong Fan, Bin Liang, Jianchun Cheng, and Yun Jing, “Ultrathin acoustic metasurface-based schroeder diffuser,” *Phys. Rev. X* **7**, 021034 (2017).
 - 32 Andrey N Tikhonov and Vasilij Y Arsenin, “Solutions of ill-posed problems,” New York , 1–30 (1977).
 - 33 David Colton and Rainer Kress, *Inverse acoustic and electromagnetic scattering theory*, Vol. 93 (Springer Nature, 2019).
 - 34 Salvatore Torquato, “Inverse optimization techniques for targeted self-assembly,” *Soft Matter* **5** (2008), 10.1039/b814211b.
 - 35 G. Zhang, F. H. Stillinger, and S. Torquato, “Probing the limitations of isotropic pair potentials to produce ground-state structural extremes via inverse statistical mechanics,” *Phys. Rev. E* **88**, 042309 (2013).
 - 36 Alberto Franceschetti and Alex Zunger, “The inverse band-structure problem of finding an atomic configuration with given electronic properties,” *Nature* **402**, 60–63 (1999).
 - 37 Mikael C. Rechtsman, Frank H. Stillinger, and Salvatore Torquato, “Optimized interactions for targeted self-assembly: Application to a honeycomb lattice,” *Phys. Rev. Lett.* **95**, 228301 (2005).
 - 38 Mikael Rechtsman, Frank Stillinger, and Salvatore Torquato, “Erratum: Optimized interactions for targeted self-assembly: Application to a honeycomb lattice [phys. rev. lett. 95, 228301 (2005)],” *Phys. Rev. Lett.* **97**, 239901 (2006).
 - 39 Mikael Rechtsman, Frank Stillinger, and Salvatore Torquato, “Designed interaction potentials via inverse methods for self-assembly,” *Phys. Rev. E* **73**, 011406 (2006).
 - 40 Mikael Rechtsman, Frank Stillinger, and Salvatore Torquato, “Erratum: Designed interaction potentials via inverse methods for self-assembly [phys. rev. e 73, 011406 (2006)],” *Phys. Rev. E* **75**, 019902 (2007).
 - 41 Mikael C. Rechtsman, Frank H. Stillinger, and Salvatore Torquato, “Synthetic diamond and wurtzite structures self-assemble with isotropic pair interactions,” *Phys. Rev. E* **75**, 031403 (2007).
 - 42 Obioma U. Uche, Frank H. Stillinger, and Salvatore Torquato, “Constraints on collective density variables: Two dimensions,” *Phys. Rev. E* **70**, 046122 (2004).
 - 43 Eli Chertkov, Robert A. DiStasio, Ge Zhang, Roberto Car, and Salvatore Torquato, “Inverse design of disordered stealthy hyperuniform spin chains,” *Phys. Rev. B* **93**, 064201 (2016).
 - 44 Sbalzarini IF Müller CL, “Energy landscapes of atomic clusters as black box optimization benchmarks,” *Evol Comput* **20**, 543–573 (2012).
 - 45 Henry Cohn and Abhinav Kumar, “Algorithmic design of self-assembling structures,” *Proceedings of the National Academy of Sciences* **106**, 9570–9575 (2009),

- <https://www.pnas.org/content/106/24/9570.full.pdf>.
- ⁴⁶ Avni Jain, Jeffrey R. Errington, and Thomas M. Truskett, “Inverse design of simple pairwise interactions with low-coordinated 3d lattice ground states,” *Soft Matter* **9**, 3866–3870 (2013).
- ⁴⁷ Gus L. W. Hart, Volker Blum, Michael J. Walorski, and Alex Zunger, “Evolutionary approach for determining first-principles hamiltonians,” *Nature Materials* **4**, 391–394 (2005).
- ⁴⁸ Volker Blum, Gus L. W. Hart, Michael J. Walorski, and Alex Zunger, “Using genetic algorithms to map first-principles results to model hamiltonians: Application to the generalized ising model for alloys,” *Phys. Rev. B* **72**, 165113 (2005).
- ⁴⁹ A. Håkansson, J. Sánchez-Dehesa, and L. Sanchis, “Acoustic lens design by genetic algorithms,” *Phys. Rev. B* **70**, 214302 (2004).
- ⁵⁰ Andreas Hakansson, Francisco Cervera, and Jose Sanchez-Dehesa, “Sound focusing by flat acoustic lenses without negative refraction,” *Applied Physics Letters* **86**, 054102 – 054102 (2005).
- ⁵¹ Lorenzo Sanchis, Andreas Hakansson, Dorley Zanon, J. Bravo-Abad, and Jose Sanchez-Dehesa, “Integrated optical devices design by genetic algorithm,” *Applied Physics Letters* **84**, 4460 (2004).
- ⁵² Andreas Hakansson, Jose Sanchez-Dehesa, and Francisco Cervera, “Experimental realization of sonic demultiplexing devices based on inverse-designed scattering acoustic elements,” *Applied Physics Letters* **88**, 163506 (2006).
- ⁵³ P.A. Martin, *Multiple Scattering: Interaction of Time-harmonic Waves with N Obstacles*, Encyclopedia of mathematics and its applications (Cambridge University Press, 2006).
- ⁵⁴ L. Schwan and J.-P. Groby, “Introduction to multiple scattering theory,” *Fundamentals and Applications of Acoustic Metamaterials: From Seismic to Radio Frequency*, John Wiley & Sons, Inc. , 143–182 (2019).
- ⁵⁵ Victor Garcia-Chocano, Lorenzo Sanchis, Ana Díaz-Rubio, J. Martinez-Pastor, Francisco Cervera, Rafael Llopis-Pontiveros, and Jose Sanchez-Dehesa, “Acoustic cloak for airborne sound by inverse design,” *Applied Physics Letters* **99** (2011), 10.1063/1.3623761.
- ⁵⁶ Jean Boulvert, Théo Cavalieri, Josué Costa-Baptista, Logan Schwan, V. Romero-García, Gwenaél Gabard, E.R. Fotsing, Annie Ross, Jacky Mardjono, and Jean-Philippe Groby, “Optimally graded porous material for broadband perfect absorption of sound,” *Journal of Applied Physics* **126**, 175101 (2019).
- ⁵⁷ Zeki Hayran, Ramon Herrero, Muriel Botey, Hamza Kurt, and Kestutis Staliunas, “Invisibility on demand based on a generalized hilbert transform,” *Phys. Rev. A* **98**, 013822 (2018).
- ⁵⁸ Richard Taillet, *Optique Physique. Propagation de la lumière*, p. 144 (De Boeck, 2006).
- ⁵⁹ The coordinates of these distributions of points are provided in the Supplementary Material.
- ⁶⁰ N. David Mermin and N. W. Ashcroft, *Solid State Physics* (Harcourt College Publishers, New York, 1976).
- ⁶¹ S. Torquato, *Random Heterogeneous Materials: Microstructure and Macroscopic Properties*, Interdisciplinary Applied Mathematics (Springer New York, 2005).
- ⁶² Salvatore Torquato and Frank H. Stillinger, “Local density fluctuations, hyperuniformity, and order metrics,” *Phys. Rev. E* **68**, 041113 (2003).
- ⁶³ The coordinates for these distribution of points can be found in the supplementary material.
- ⁶⁴ Charles Kittel, *Introduction to Solid State Physics* (Wiley; 8 edition (November 11, 2004), 2004).